Radial Glial from mammalian developing neocortex can perform symmetric proliferative divisions in vitro

Mario Ledesma-Terrón[1], **Nuria Peralta-Cañadas**[1], **and David G. Míguez**[1]

[1]Departamento de Física de la Materia Condensada, Centro de Biología Molecular Severo Ochoa, CBMSO, Instituto de Física de la Materia Condensada, IFIMAC, Instituto Nicolás Cabrera, INC, Universidad Autónoma de Madrid, 28012, Spain, Corresponding author: David G. Míguez

This manuscript was compiled on October 28, 2019

Radial Glial progenitors in the mammalian developing neocortex have been shown to follow a deterministic differentiation program restricted to an asymmetric only mode of division. This feature contrasts with previous studies and with other developmental systems, such as the developing spinal cord, the retina, epidermis, airway epithelium, germline, and the intestine, where differentiation takes place based on probabilities that can change overtime and other modes of division are possible. Here, we combine experimental, computational and theoretical tools to show that Radial Glial cultured *in vitro* can divide symmetrically, and that the balance between the different modes of division, as well as the cell cycle length, can be modulated by external signals, such as Fibroblast Growth Factor. Our results suggest that the constraint of deterministic and asymmetric mode of division that Radial Glia exhibit in vivo may not be an inherent property of this particular cell type, but a feature induced by the complex organized pseudo-stratified structure of the mammalian developing neocortex.

cell cycle | differentiation | Branching Processes | Radial Glial | Thymidine analogs assays

The neocortex constitutes the main part of the mammalian brain, and the location where the processing of all higher-order brain functions resides. Understanding its formation is one of the major interests of Developmental Biology (1). The neocortex develops from a stratified neuroepithelium, called the neural tube, into a complex structure of six horizontal layers of excitatory and inhibitory neurons (2). Neurogenesis in the developing neocortex initiates when neuroepithelial progenitors transform into Radial Glial (RG) progenitor cells and start to produce neurons and intermediate neuronal precursors (3, 4). Since the discovery that RG constitute the progenitors of potentially all neurons in the vertebrate neocortex (5–8), a great effort has been focused in identifying their features and properties: how they coordinate in time and space to form the multiple layers of the neocortex?; which signals control their fate?; and how these signals orchestrate the correct balance between proliferation or differentiation during neurogenesis?.

In principle, this balance can be robustly achieved via stochastic or deterministic cell decisions (9). In brief, stochastic models assume certain probability of differentiation that depends on the intracellular and extracellular signals that the cell is receiving. In this context, the fate at the single cell level is unpredictable and the balance between proliferation and differentiation is regulated at the level of the population (10). On the other hand, deterministic models of stem cell differentiation assume that the fate of the progeny is fixed and, therefore, the correct balance between the numbers of different types of neurons is achieved at the single cell level (11).

The dynamics of differentiation is often characterized based on the fate of the two daughter cells of a cell division relative to each other (12). This way, proliferating progenitors can perform *pp* (progenitor-progenitor), *pd* (progenitor-differentiated) and *dd* (differentiated-differentiated) divisions (13).

In this context, differentiation in the developing chick spinal cord (14), in the zebrafish retina (15, 16), epidermis (17), airway epithelium (18), germline (19), and the intestine (20) of mice follow an stochastic model. In these systems, progenitors can potentially perform each of the three types of division, and the corresponding rates are probabilistic and change overtime. On the other hand, the differentiation of RG in the mammalian brain has been shown to follow a deterministic asymmetric-only mode of division (3, 21), contradicting previous studies that show a small but non-negligible percentage of symmetric proliferative divisions *in vivo* (8, 22)

The important differences between the deterministic mode of division proposed in ref. (21) compared to other neurogenic tissues, and the discrepancy with previous studies (8, 22) suggested us to further investigate the dynamics of mode and rate of division of RG. To do that, we quantified the proliferation and differentiation *in vitro* cultures, where environmental conditions are fully controlled and constant. Previous studies of *in vitro* RG cultures (23) show mainly asymmetric divisions, based on the self-renewing potential of the progeny (and

Significance Statement

It is well established that, during the neurogenesis of the mammalian neocortex, Radial Glial can only divide asymmetrically. To understand the features that set this important restriction, we analyze *in vitro* cultures from mouse developing neocortex during the differentiation of Radial Glial into terminally differentiated neurons. Our results show that Radial Glial cultured *in vitro* also divide symmetrically. Moreover, the balance between the division modes can be modulated by external signals, such as Fibroblast Growth Factor. In conclusion, our results suggest that the constraint of deterministic and asymmetric mode of division of Radial Glial is not an inherent property of this particular cell type, but a feature induced by the complex organized pseudo-stratified structure of the mammalian developing neocortex.

MLT performed research and wrote the manuscript, NPC, perfomed reserach, DGM designed research, performed research and wrote the manuscript.

Authors declare no competing interests.

[2]To whom correspondence should be addressed. E-mail: david.miguezuam.es

DRAFT

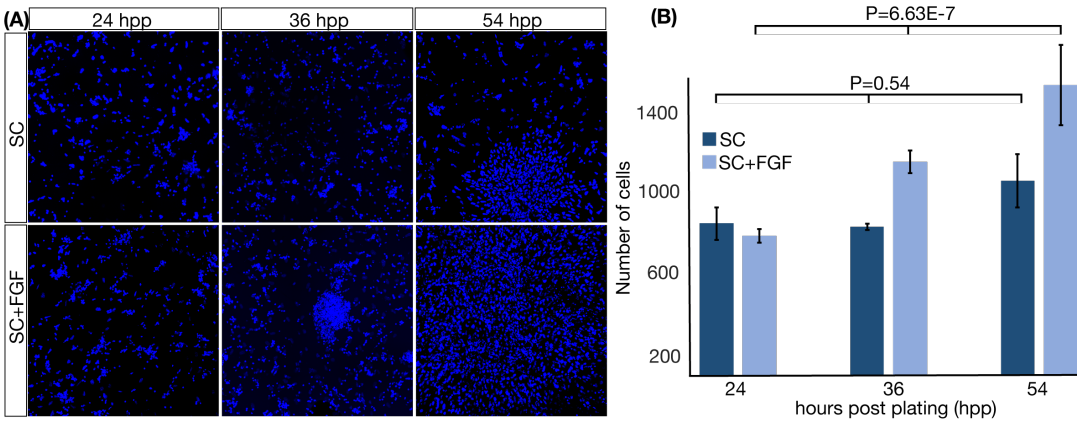

Fig. 1. The growth rate of the population of RG can be modulated by FGF stimulation. (A) Snapshots of RG cultures at different hours post plating (hpp) stained with Hoechst and growing at SC and SC+FGF culture conditions. (B) Quantification of total cell numbers in a field of view of 0.6 mm $\times$ 0.6 mm at different time points shows that only cells in SC+FGF stimulation increased in number with statistical significance ($P < 0.05$). Error bars correspond to standard error of the mean value between multiple samples of similar conditions.

not based on the fate of the daughter cells as proliferative or terminally differentiated (13)).

Our approach combines experimental, computational and theoretical tools where *in vitro* cultures of RG from mouse developing cerebral cortex grow at different conditions. Quantitative values of cell numbers at different time points are then used to inform a theoretical framework based on a branching process formalism (14). Our results show that RG are able to divide both symmetrically and asymmetrically when cultured *in vitro*, and that the average mode of division changes overtime, as well as the average cell cycle length (14). In addition, the mode of division and the length of the cell cycle can be modulated by external cellular signals, such as Fibroblast Growth Factor (FGF). Our results suggest that the deterministic mode of differentiation or RG reported *in vivo* (3, 21) is not an intrinsic property of the cells, and therefore, it may be imposed by the spatio-temporal restrictions provided by the stratified organization of the developing neocortex.

Results

RG proliferate in culture at a rate dependent on FGF stimulation. To initially test if the dynamics of RG growth and differentiation *in vitro* recapitulate *in vivo* observations, cells derived from the developing neocortex of mouse embryos at E11-11.5 are extracted, plated and cultured following standard protocols (24). Starting at 24 hours post plating (hpp), samples are then fixed at three different time points and stained with Hoechst (Fig. 1A). Quantification of the number of cells in a field of view of fixed dimensions using an automated segmentation tool (see Supplementary Methods) is shown in Fig. 1B for two culture conditions: SC and SC+FGF, where the standard culture media is supplemented with an increased concentration of FGF basic ligand (see Methods). In both conditions, the number of cells increases, but the growth is only statistically significant ($P < 0.05$) in SC+FGF conditions.

It has been shown previously that the fate of differentiating RG can be modulated by external signals. For instance, FGF2 has been shown to alter the differentiation progeny of RG from neurons to glia (25). In addition, Wnt signaling has been shown to regulate the potential to generate the different neuronal subtypes of RG (26). Our results suggest that externals signals such as FGF can also modulate the growth rate of the population of RG *in vitro*.

FGF stimulation of RG cultures result in shorter cell cycle length. In principle, increased growth rate in a differentiating stem cell population can be caused by changes in the number of cycling cells, reduced cell death, reduced differentiation rate or a direct effect in the cell cycle dynamics. To study how FGF affects the dynamics of growth of the population of RG in culture, we perform 5-ethynyl-2'-deoxyuridine (EdU) cumulative labeling experiments to measure changes in the length of the average cell cycle.

BrdU (27), EdU (28, 29) and other thymidine analogs constitute the most used tool to estimate the cell cycle length of cells in many contexts (30). The methodology is based on the replacement of endogenous thymidine during DNA synthesis with traceable compounds (31, 32). The length of the average cell cycle is then inferred from the dynamics of the incorporation of these compounds into the DNA of cycling cells using well established methods (33).

To estimate the average cell cycle length of the population, samples are cultured in the presence of EdU and then fixed at different time points (corresponding to different times of EdU incorporation). Combined nuclear Hoechst staining with EdU detection assay and immunostaining against Sox2 is used to identify all progenitors that have passed through S-phase for each EdU incubation time.

The cell cycle length T and the growth fraction γ are calculated using the standard cumulative curve methodology based on linear regression (see Methods). Results are shown in Fig. 2. The data (Figs. 2C,D) reveals that γ remains at around 72% for both conditions tested, while T depends strongly on the culture conditions (T=35.2 $\pm$ 3.5 hours for SC, T= 24.7 $\pm$ 2.0 hours for SC+FGF). In conclusion, our results show that FGF stimulation shortens the average cell cycle length in cultures of RG *in vitro*.

EdU-estimated cell cycle values in conditions of asymmetric-only mode of division does not reproduce the experimental observations. Next, we ask whether the values of cell cycle length measured with EdU cumulative labeling can account for the dynamics of the population of RG observed in Fig

DRAFT

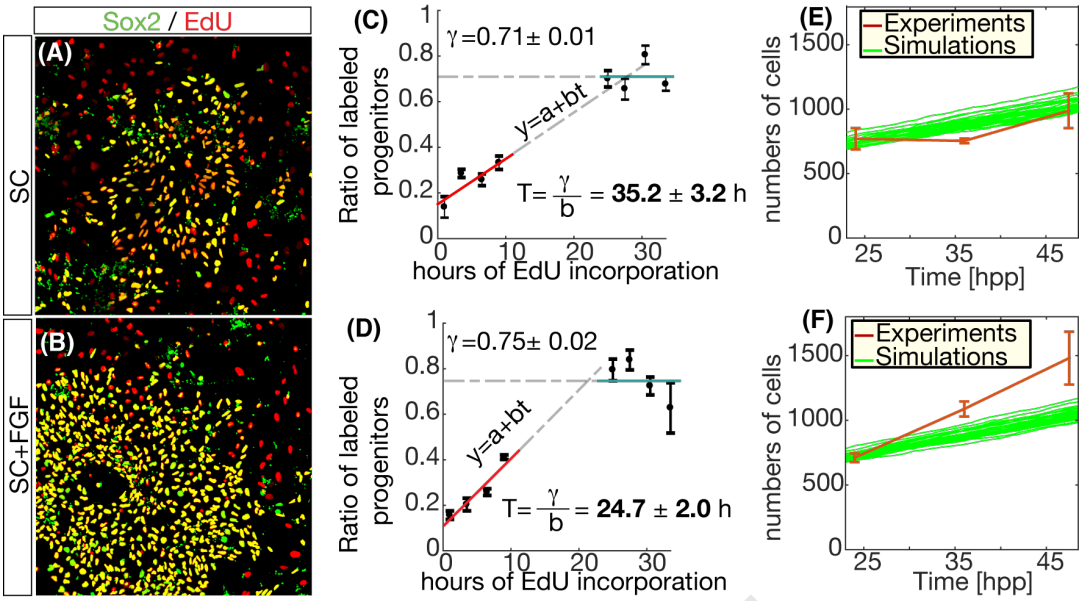

Fig. 2. Increased FGF results in shortening of the division time of cycling RG. (A-B) Snapshots of *in vitro* cultures stained with Sox2 (green) to label RG and EdU (red) to label cells that have gone through S-Phase after 24 hours of EdU incorporation. (C-D) Cumulative curve quantification of EdU positive progenitors in the culture versus EdU incubation time. Cells in SC+FGF conditions cycle faster (T= 24.7 $\pm$ 2.0 hours) than in SC (T=35.2 $\pm$ 3.5 hours). The growth fraction γ is similar for both conditions (around 0.72). (E-F) Numerical simulations of a model of cycling and differentiating RG (green lines) show that the experiments (red data points) fit with a scenario with constant cell cycle and restricted asymmetric division of the RG for control condition, but not for SC+FGF conditions.

DRAFT

1B. To do that, we developed a computational model of a generic differentiating stem cell population that simulates cycling progenitors that can either proliferate, differentiate, enter quiescence or apoptosis based on rates and probabilities provided by the user. Values of cell cycle length, mode of division, quiescence and death rate can be kept constant throughout the simulation, or can be set to change each time-step. Parameters are sampled from a gamma distribution to mimic intrinsic cell-to-cell variability. Details of the model are presented in the Supplementary Methods section. A scheme of the simulation framework is shown in Supplementary Figure S1.

The model is then informed with the values of initial number of cells, cell cycle T and growth fraction γ measured in the previous section (apoptosis rate is set to zero). Following the recent literature on RG proliferation and differentiation dynamics (3, 21), the division mode is restricted to deterministic and asymmetric *pd*. Results are shown in Fig. 2E,F for 30 independent numerical simulations (green lines). The dynamics of the SC conditions closely resembles the experimental data (red), while in extra SC+FGF conditions, the population grows at significantly lower rate than the experimental *in vitro* culture.

In conclusion, the numerical model shows that the values of cell cycle length obtained by cumulative EdU labeling and the hypothesis of asymmetric differentiation do not explain the increased in the total number of cells observed in SC+FGF conditions.

Comparison between different methods to monitor cell cycle dynamics show inconsistent values. The use of thymidine analogs to measure cell cycle dynamics has several drawbacks: it can be toxic and mutagenic (34) and affect the normal dynamics of cell proliferation (35) by lengthening the cell cycle. In addition, choosing the correct mathematical analysis and interpretation of the experimental data is not straightforward (36). Authors have proposed several approaches, such as linear (37, 38), nonlinear fitting (39, 40), or the use of deterministic (41) or stochastic models (42). Depending on the method used, the same input data results in quite different predictions for the average duration of the cell cycle (43). Due to these limitations, BrdU and analogs have been referred as "one of the most misused techniques in neuroscience" (44).

To try to understand why the data of cell cycle length provided by EdU in the previous section does not predict the dynamics of the population in SC+FGF conditions, the previous numerical model is modified to simulate EdU labeling (cells in S-phase are marked as labeled when EdU is present). Then, the number of progenitors, differentiated and EdU positive progenitors at each time point is used to calculate the average cell cycle length of the population using three widely used EdU based methods: single cumulative curve (C1) (27), dual cumulative (C2) (45), and the pulse-chase (PC) method (40) . The cell cycle is also calculated using the branching process (BP) method introduced in Ref. (14) (see Supplementary Methods). A detailed description of each method and how it is applied in this context is illustrated in Supplementary Figure S3 and explained in the Supplementary Methods section. All predictions are then compared with the input value of T used for each simulation, to estimate the accuracy and reliability of each method.

The first scenario tested corresponds to homeostasis in the progenitor population ($pp - dd$=0), constant value of T=20 hours and no quiescent or apoptotic cells ($\gamma = 1, \emptyset_P = 0$). These are the conditions defined by Nowakowski and coworkers when introducing the cumulative curve method (27). Results of the analysis are plotted in Fig. 3A. Dots in Fig. 3B correspond to the prediction of the value of T for 10 independent simulations (crosses represent the average). We see that, for

these particular settings, all four methods are able to predict the correct value of T (dashed line) within a 10% error margin, with both PC and BP performing slightly better than C1 and C2. Importantly, the values predicted by the 10 simulations for the two cumulative methods show a high dispersion. This suggests that a high number of repeats should be necessary to get an accurate value of T (the typical experimental design that involves only three independent repeats does not guarantee a correct estimation of the cell cycle). The same conclusions apply when considering growth of the population of progenitors ($pp - dd > 0$, Supplementary Figure S4A).

Variable cell cycle dynamics has been reported in many developmental systems (14, 46–56). Fig. 3C shows the output of the numerical model when a variable value of T is used as input (with an average value T= 20 hours). Fig. 3D plots the quantification of the cell cycle in these conditions. In this situation, C1 predicts a much longer cell cycle that the average (49% error), while the C2 predicts a shorter cell cycle (24% error). Interestingly both PC and BP return a value much closer to the correct average, with less than 10% error. Again, the variability of the cumulative methods is very high, making them unreliable methods when a small number of repeats are used. Again, the same conclusions apply when considering conditions where the cell cycle changes while the population of progenitors is allowed to grow ($pp - dd > 0$, Supplementary Figure S4B).

The balance between differentiative and proliferative divisions has been shown to also change overtime in many developmental systems (14, 46). For instance, during motorneuron generation, the rate of differentiation changes rapidly due to a sudden switch in Shh levels (46). When we set a variable differentiation rate in our simulations, we observe that again both cumulative methods fail and show high dispersion between independent samples (Supplementary Figure S4C). The same occurs when both mode and rate of division are allowed to change simultaneously (Supplementary Figure S4D).

In conclusion, these results show that methods based on cumulative curve labeling are not suitable when proliferation and/or differentiation rates are not constant. This, together with the reported effect of BrdU and analogs in lengthening the cell cycle, could explain the discrepancy between simulations and experiments shown in Fig. 2E-F. In addition, the branching formalism is more accurate and has the advantage of providing values of the average mode of division, also with temporal resolution.

FGF stimulates the generation of progenitors in culture. Based on the observations in the previous section, the branching process formalism is now used to measure the proliferation and differentiation dynamics of the RG population. To do that, samples are cultured starting at 24 hpp and fixed every 2-4 hours. Next, samples are stained using antibodies against Sox2 and Map2 to identify progenitors and differentiated cells, respectively. We then identify the fate of each cell based on the intensity of Sox2 and Map2 staining using our segmentation framework in images of 0.6 mm × 0.6 mm (see Supplementary Methods).

Results are shown in Fig. 4 for the two conditions tested: SC and SC+FGF. Output provided by the segmentation script is plotted in Figs 4B,C. Assuming the typical logistic growth model (57) for proliferating cells in cultures and negligible cell death (see Supplementary Figure S2A and ref. (22)), the

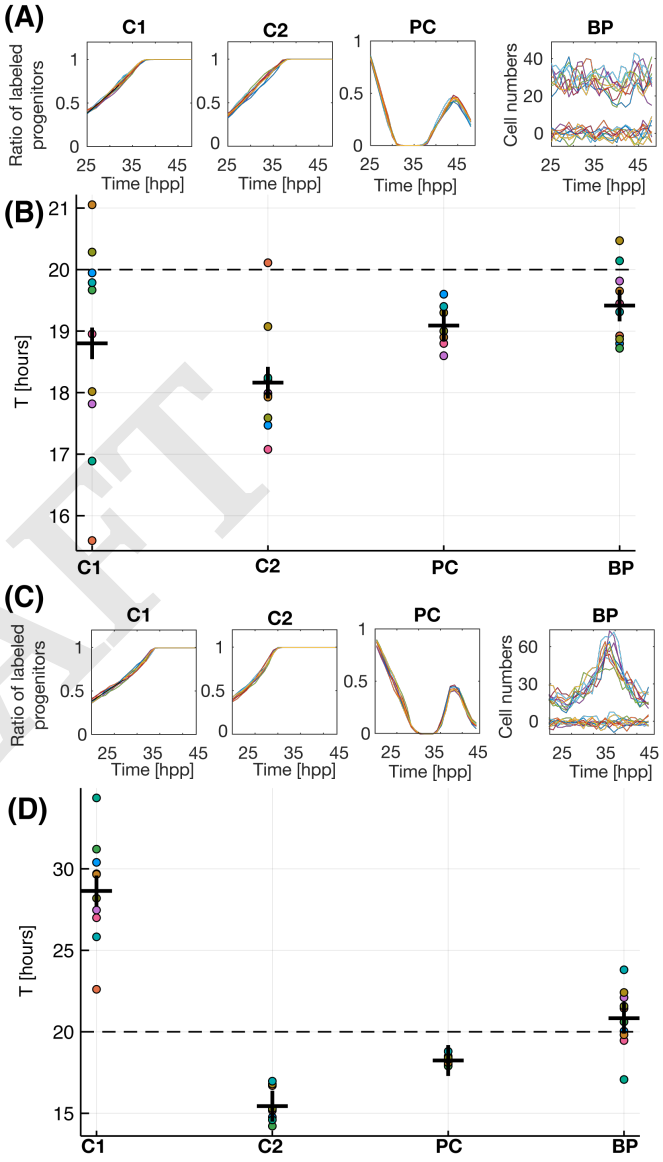

Fig. 3. Simulations explain the difference in cell cycle length calculated by EdU and Branching process. (A,C) Cumulative curves generated numerically for each protocol for 10 independent runs of the model. (B,D) Quantification of T for each simulation (dots) and average (crosses). Each color corresponds to the same simulation analyzed using each framework. A-B correspond to conditions of constant cell cycle. C-D correspond to conditions of variable cell cycle.

DRAFT

corresponding sigmoidal curve fitting is also plotted (green, red, and blue lines for RG, neurons and total cells, respectively). The data shows that an initial regime of reduced change in cell numbers is followed by an increase in both cell types until the system reaches a regime where few new cells are being generated. In both conditions, the amount of progenitors (green data points, green line) and differentiated cells (red data points, red line) increases with statistical significance ($P < 0.05$) but the increase in progenitors is statistically more significant in conditions of SC+FGF (P= 7.25E-09) that in SC conditions (P= 7.60E-03).

To rule out the possibility that this increase is due to the presence of early neuroepithelial progenitors in the culture (that proliferate only via *pp*) (3, 4), we performed immunofluorescence against Pax6, a well characterized marker for RG (58) that is not present in neuroepithelial progenitors (59). Quantification is shown in Supplementart Figure S5, where around 100% of all Sox2 positive progenitors are also positive for Pax6 (so, there is no neuroepithelial progenitors at this stage in the culture, in agreement with the in *in vivo* data (3)). Another possibility is the presence of intermediate progenitors (60) that divide once to produce two terminally differentiated neurons (61). Immunofluorescence against Tbr2, a marker for intermediate progenitors shows that no Tbr2 positive cells in the culture in the two culture conditions tested (data not shown). This is probably due to the fact that FGF has been shown to inhibit the transition from RG to intermediate progenitor (62) (FGF is in the culture media in both experimental conditions: SC and SC+FGF).

In conclusion the addition of FGF results in more progenitors and similar number of differentiated cells, and not an increase in one population to the expenses of the other. This is consistent with a reduced cell cycle length after FGF increase. Nonetheless, the increase in the number of progenitors is inconsistent with the observation that RG from mouse neocortex can only divide asymmetrically *in vivo* (3, 21) (in this scenario, the total amount of RG cells should remain constant or close to a constant value).

Branching process formalism predicts variable mode and rate of division. The previous observation suggests that, apart from the changes in the cell cycle length, FGF is also affecting also the mode of division of the RG. When the fitted values of cell numbers for progenitors and differentiated cells from the previous section are used as input of the branching process equation for T (Eq. 2 in the Supplementary Methods section) we obtain the average cell cycle length (Fig. 5A). Results show that average T is not constant: a sharp decrease in cell cycle length is followed by a sharp increase at later time points. Interestingly, the minimum of the cell cycle for SC (around $T = 19$ hours) and SC+FGF (around $T = 10$ hours) conditions both occur around 36-37 hpp. These values are close to the values shown *in vivo* in Refs. (3, 21), that measured an average cell cycle length of 16-18 h in the temporal window corresponding to E11-E13.

Fig 5B shows the prediction for the average mode of division *pp-dd* (Eq. 1 in the Supplementary Methods section). In both cases, differentiation appears to increase in time, and this change is reduced in SC-FGF conditions.

Interestingly, both situations show values of $pp - dd$ different from the value that corresponds to a restricted asymmetric differentiating mode ($pp - dd = 0$, i.e., $pd = 1$). In addition, the maximum change in the differentiation dynamics occurs around 36-37 hpp, coinciding with the minimum of T of both conditions. In conclusion, quantification of the cell numbers using the branching process framework suggest that the presence of FGF in the culture media speeds up the cell cycle time while also reducing the differentiation rate. Interestingly, our data also shows an increase in the growth fraction γ in conditions of SC+FGF compared to SC, when monitoring the cycling progenitors using KI67 staining (Supplementary Figure S2C-D), in agreement with previous studies (63).

Values from the branching process analysis are able to reproduce the experimental data. To test if the values provided by the branching process formalism are correct, we take advantage of the same numerical model of the differentiating stem cell population introduced previously. Now, the model is informed with the prediction of T and $pp - dd$ plotted in Fig. 5A-B. The growth fraction and apoptosis rate are also obtained from the experimental data in Supplementary Figure S2. Results are plotted in 5C-D, where we plot the prediction for number of progenitors and differentiated cells (thin green and red lines, respectively) for 30 independent simulations. Comparison with the fitting of the experimental data for progenitors and differentiated cells (thick green and red lines, respectively) show a good agreement in both conditions, suggesting that the branching equations are able to predict the correct average mode and rate of division of RG *in vitro*.

The number of RG labelled after a short EdU pulse increases in time. To further validate the outcome of the branching process formalism that predicts a non negligible number of *pp* divisions, we designed an experiment based on Pulse-and-Chase of EdU labelled cells. Do do that, we plate cells from mouse developing neocortex following the procedure explained in Methods section. Next, cells are cultured in SC and SC+FGF conditions until 33 hpp (when T is fastest, Fig. 5A). At this point, a pulse of 30-minutes of EdU is applied to all samples. A number of samples are fixed at this time point (and labeled as "Pulse" time point). The rest of samples are washed with fresh culture media 5 times to remove the Edu (see Methods). These samples are cultured for another 15 hours (corresponding to the predicted average T for SC+FGF conditions during this time, to ensure that labeled cells cannot cycle more than once in any of the culture conditions). Next, cells are fixed and stained with Hoechst, EdU and Sox2 immunostaining. Finally, the number of Sox2+/EdU+ cells at the time of the pulse (33 hpp) and chase (47 hpp) is quantified using our automated image analysis tool (see Supplementary Methods). Results are shown in Fig. 6. The number of progenitors labeled with EdU does not change significantly in SC conditions, consistent with a large proportion of asymmetric divisions (i.e, one EdU+ RG produces two EdU+ cells: one RG and one neuron, so the amount of EdU+ RG remains constant). On the other hand, in conditions of SC+FGF, we see a statistically significant (P<0.05) increase in the number of EdU+ RG when comparing "pulse" and "chase" time points. This result shows that some of the RG originally labeled with the short EdU pulse, divided and produced more than one RG per division, showing that, as predicted by the branching formalism, RG are capable to undergo symmetric proliferative pp divisions *in vitro*.

DRAFT

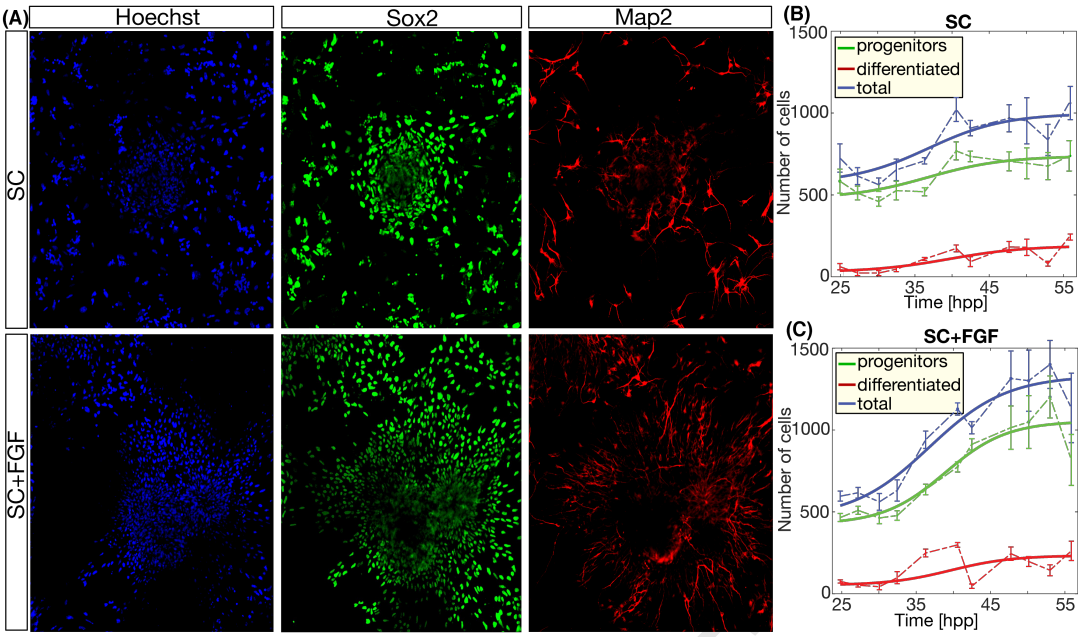

Fig. 4. FGF stimulation increases the amount of progenitor cells. (A) Snapshots of RG cultures at 24 hours post plating showing nuclei (Hoechst), progenitors (stained with Sox2) and differentiated neurons (stained with Map2). (B-C) Quantification of the number of cells of each type in both culture conditions shows an increased number of progenitors is SC+FGF, compared to SC conditions. Error bars correspond to standard error of the mean. Lines correspond to nonlinear sigmoidal fitting of the experimental data points.

DRAFT

Discussion

A detailed analysis of the dynamics of vertebrate neurogenesis involves a careful characterization of the features that regulate the dynamics of proliferation and differentiation of RG during the generation of the mammalian cortex. One of its most striking features is the fact that RG are restricted to an asymmetric mode of division *in vivo*, in contrast with previous observations (8, 22) and with other developmental systems (14–20, 46). Our study suggests that RG are not restricted to an asymmetric mode of division when cultured *in vitro*, and that symmetric proliferative *pp* divisions are taking place during the temporal window analyzed. In addition, we show that extracellular signals do not only affect the type of progeny (25, 26) during RG differentiation, but can also modify strongly the length of the cell cycle (Fig. 5A), the mode of division (Fig. 5B), or the rate of quiescence of RG (Supplementary Figure S2C-D).

Several authors propose that the mode of division depends on the distribution of cell fate determinants during mitosis, the orientation of the spindle or the inheritance of the primary cilium or the different centrosomes (4). It is possible that the apical-basal polarized structure of the RG, or their organization and orientation of the radial processes along the stratified neuroephitelium results in asymmetric inheritance of these cell fate regulators (4). The loss of these polarizing features provided by the niche when cells are cultured *in vitro* may result in a probabilistic scenario where the fate of the two daughter cells is independent of each other and all of the 3 modes of divisions are possible, similarly to neuronal progenitor cells and other developmental systems (14–20, 46). In fact, early studies in the mouse neocortex suggest that the model that fits best the clone distribution assumes that the fate of the daughter cells is independent of each other (22). In this situation, the branching process framework is able to estimate the rates of each of the three modes of division (14). This prediction for the case of RG in culture is shown in Fig. 5E-F, where we can see that the predominant mode of division is *pp* (green). This symmetric mode of division is even more probable in conditions of SC+FGF, to the expenses of a reduction in *pd* and *dd*. A scheme that illustrates our findings is shown in Fig 6C. In brief, the single mode of division observed *in vivo* contrast with the probabilistic scenario observed *in vitro*, where all modes of division are possible. Changes in the culture conditions can shift the balance between the three modes of division, and increase the rate of *pp* divisions to the expenses of the other modes.

A detailed analysis of the dynamics of vertebrate neurogenesis involves a careful characterization of the rate of division. The most direct method to measure the cell cycle length requires to monitor the time between consecutive mitotic evens at single cell resolution (64). Unfortunately, due to the high degree of variability, many cells in a population need to be sampled, segmented and tracked simultaneously to obtain an accurate value, even when dealing with clonal samples (65).

Indirect methods based on cumulative incorporation of thymidine analogs perform well in conditions of constant proliferation and differentiation, but they are not designed to study systems where the cell cycle changes overtime, which is is potentially the case in many developmental systems. In these conditions, the Branching Process formalism and the Pulse-Chase outperform cumulative curve methods. On the other hand, the Pulse-Chase method requires experiments that are longer that cell cycle length. Therefore, the toxic effect of the labeling agent for long periods of time may affect strongly the normal cell cycle progression (34, 35). A clear advantage of the Branching Process is that it does not involve manipulation of the samples before fixation, so there is no interference

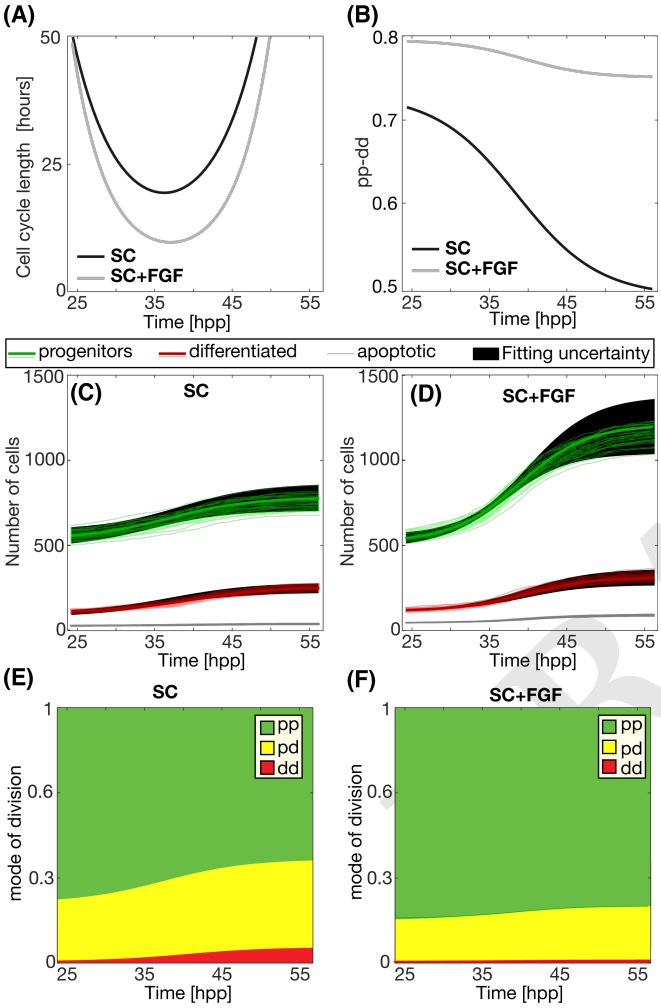

Fig. 5. FGF affects the proportion of symmetric proliferative divisions in RG culture (A-B) Plot of the average T (A) and $pp - dd$ of the population of RG under SC (black) and SC+FGF (grey) conditions. (C-D) Simulations (light red and green lines) for both conditions using parameters of mode and rate of division of (A-B). Thick lines correspond to the sigmoidal fitting of the experimental data in Fig. 4. Black regions mark the uncertainty derived from the fitting. (E-F) Prediction for each mode of division using a stochastic model of differentiation.

with the normal progression of the cell cycle. In addition, the Branching Process formalism also provides the correct value of T with temporal resolution, and the measurement of the average differentiation rate, (also with temporal resolution).

Several studies have shown that the length of G1 phase increases progressively when neurogenesis starts, resulting in a overall increase of the cell cycle (48–53). Alternatively, others studies show that the cell cycle length is shorter in neurogenic divisions, compared to proliferative divisions (46, 47, 54–56), due mainly to a shortening in S-phase. Our results show that FGF promotes pp divisions and shortens cell cycle, consistent with the hypothesis that proliferative divisions have a shorter cell cycle, maybe via a shortening of G1-phase (similarly to insulin-like growth factor (66, 67)). A careful characterization of how FGF affects each phase of the cell cycle it is far from the scope of this contribution.

The culture and differentiation of RG cells *in vitro* provides a very good framework to study basic features that orchestrate the formation of the mammalian neocortex. In brief, the system provides a well controlled environment where the effect of signaling molecules and other conditions can be tested reliably, while providing easier manipulation and imaging compared to studies performed *in vivo*. We use this framework to study the features that restrict the division mode of RG as deterministic versus the more common probabilistic scenario observed in many other scenarios. Our combined experimental/computational/theoretical approach can be also used to test the effect of other signaling networks by quantifying the cell cycle and mode of division after small molecule inhibition and comparison with a control culture.

Acknowledgements

We thank professor Francisco Wandosell for multiple discussions and invaluable input at all stages of this work. Research was funded via grants BFU2014-53299-P and RTI2018-096953-B-I00 from the Ministerio de Ciencia, Innovación y Universidades (Spain). ML has been funded via Instituto de Física de la Materia Condensada (IFIMAC) of the Universidad Autónoma de Madrid with an FPI grant.

Supporting Information Appendix (SI). Additional figures and Methdos are provided as Supporting Information

Materials and Methods

Preparation and culture of dissociated mouse cortical RG. Cells were obtained from mouse embryos of the C57 BL/6JRCC line at E11/E11.5, following standard methods described previously (see Ref. (24)). The initial time point is labeled as 0 hours post plating (hpp) and it is used as the reference point for our experiments. Briefly, after careful removing of the meninges, the cortex is isolated and placed in Hank's Buffered Salt Solution free of Ca2+ and Mg2+ (HBSS, ThermoFisher 14185). Next, samples are mechanically disgregated using Pasteur pipettes and plated in coverslips treated with Nitric Acid and Fibronectin at 10 µg/ml (Fisher Scientific; 15602707) to facilitate cell adhesion. Cells are plated at constant density (250000 cells in each M24 well) for all experiments in Neurobasal medium without L-glutamine (ThermoFisher 21103-049), Glutamax (ThermoFisher 35050-038), B-27 (ThermoFisher 17504-044) Penicillin, Streptomycin and Antimicotic (concentrations standard for cell culture). Media is complemented with 0.02 ng/μl of recombinant murine EGF (PeproTech 315-09, lot number 0517179-1) and 0.02 ng/μl of human FGF basic (PreproTech

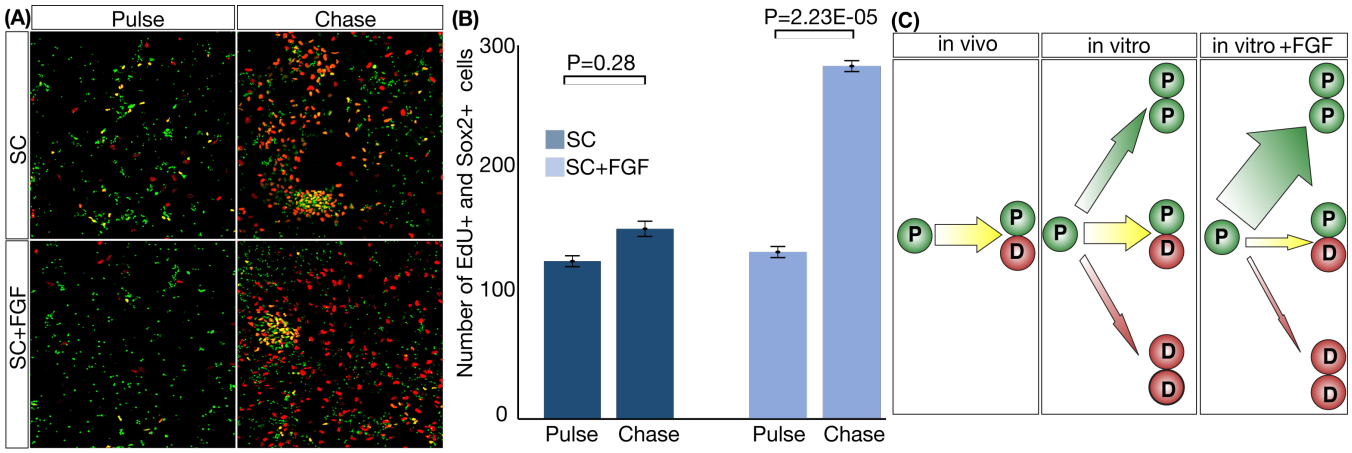

Fig. 6. Pulse-Chase experiment shows increased EdU labeled RG cells in presence of an extra concentration of FGF. (A) Representative images showing Sox2 and EdU staining in green and red, respectively. (B) Quantification of the number of Sox2 and EdU positive cells for Pulse and Chase time-points for SC and SC+FGF conditions. The number of EdU labelled RG cells increases in the Chase time-point in conditions of SC+FGF with statistical significance. Error bars correspond to standard error of the mean value between independent repeats of the experiment. (C) Scheme that summarizes the experimental observations.

100-18B, lot number 0311706-1). This culture media is referred as *standard culture* (SC) conditions in our study. Cells are allowed to rest a full day in the incubator to recover the dissection process. 24 hpp, the culture media is changed with fresh SC media, or to SC media complemented with additional human FGF basic to a final concentration of 0.06 ng/μ). This culture conditions are labeled as SC+FGF in this study. All experimental protocols were in accordance with the guidelines of the European Communities Directive (2012/63UE) and the actual Spanish legislation (RD 53/2013).

Immunofluorescence. Cells are fixed for 20 minutes at Room Temperature (RT) with 4% paraformaldehyde and washed twice for 5 minutes with Phosphate Buffer Saline 1X (PBS). Fixed cells are incubated with the permeabilization solution composed of Triton x-100 (ChemSupply 9002-93-1) at 0.6% in PBS 1X for 20 minutes at RT. Next, cells are washed 3 times with PBS and blocking solution is added (Bovine Serum Albumin, BSA. Sigma ;A7906) at 3% in PBS for at least 30 minutes. Later, cells are incubated with primary antibodies dissolved in the blocking solution overnight at 4ºC. The next day, cells are washed with PBS 3-4 times for 5 minutes, and they are incubated with secondary antibodies in the blocking solution for 45 minutes at RT, protected from light. Next, secondary antibodies are washed out (PBS 3-4 times for 5 minutes), and nuclei is stained with Hoechst 3342 (1/2000, ThermoFisher 1399) dissolved in PBS for 5 minutes at RT. Finally, cells are washed in PBS, double distilled water, and ethanol at 70%. Cover-slips are finally mounted with Fluoromount G (Southern Biotechnology Associates, Inc, Birmingham, Alabama 0100-01) on microscope glass slides. Primary antibodies used are: anti-Sox2 (1/2000, GeneTex GTX124477), anti-Map2 (1/200, Santa Cruz Biotechnology sc-74421); anti-Pax6 (1/1000, BioLegend B244573); anti-Cleaved Caspase 3 (1/1000, Cell Signaling 9661); and anti-KI67 (1/200, ThermoFisher 14-5698-82). Secondary antibodies used are: anti-Rabbit 488 (1/1000, ThermoFisher A-21206), anti-Mouse 555 (1/1000, ThermoFisher A-21137) and anti-Rat 555 (1/1000, ThermoFisher A-21434).

Statistical and Data analysis. One way ANOVA test is used to measure statistical significance between different time points. Cell cycle values in Fig. 2C-D are obtained after linear regression of the four first data points. Rates of quiescence in Fig. 2C-D are obtained from the mean value of the four last points. Slope error is calculated doing a linear fitting with values of the average plus standard error and another one with values of the average minus standard error to get the difference in the slope between these two values. Quiescence error is the standard error of the four last points, and the T error is derived from the error propagation of the previous values. Three-parameter sigmoidal fitting is used to fit data from fig. 4B-C. Black regions in Fig. 5C mark the uncertainty derived from the fitting, calculated from the difference between the result of the fitting using as values the mean plus the standard error, and the result of the fitting using as values the mean minus the standard error (with the same values of the parameters). Sample size for all experiments is at least 4. Unless specified, errorbars represent the standard error of the mean. Error values are calculated using error propagation. All curve fitting and statistical analysis are performed using Matlab© (The Mathworks©, Natick, MA).

EdU cumulative curve. Cumulative curve of the thymidine analog 5-Ethynyl-2'-deoxyUridine (EdU) incorporation is performed using Click-iT^{TM} Plus EdU Alexa Fluor^{TM} 647 Imaging Kit (ThermoFisher; C10640). Briefly, EdU was added around 24 hpp at 2 μM. Cells are then fixed at increasing times of EdU exposition. Staining of EdU positive cell is performed based on previously published protocols (68). Next, immunostaining against Sox2 is used as standard marker for RG progenitors (3). Later, the number of cells positive for both Sox2 and EdU is quantified using automated image processing. To calculate the cell cycle length, the percentage of progenitor cells that have incorporated EdU is plotted against the hours of EdU incorporation. The saturation value at long incubation times is used to calculate the growth fraction γ. This value is then used to calculate the average cell cycle using linear regression at short EdU accumulation times (see figure 2).

EdU pulse-and-chase experiments.. Cells are exposed to a short pulse of 30 minutes of EdU at 36 hpp. "Pulse" points are fixed at this time point. "Chase" points are washed three times with fresh medium and are fixed 15 hours after the "Pulse" time point. The number of EdU positive/Sox2 positive cells is quantified in both "Pulse" and "Chase" time points for both conditions using automated image processing.

ACKNOWLEDGMENTS. We thank professor Francisco Wandosell for multiple discussions and invaluable input at all stages of this work. Research was funded via grants BFU2014-53299-P and RTI2018-096953-B-I00 from the Ministerio de Ciencia, Innovación y Universidades (Spain). ML has been funded via Instituto de Física de la Materia Condensada (IFIMAC) of the Universidad Autónoma de Madrid with an FPI grant.

1. S Lodato, P Arlotta, Generating neuronal diversity in the mammalian cerebral cortex. *Annu. Rev. Cell Dev. Biol.* **31**, 699–720 (2015).
2. F Matsuzaki, A Shitamukai, Cell division modes and cleavage planes of neural progenitors during mammalian cortical development. *Cold Spring Harb. Perspectives Biol.* **7**, a015719 (2015).
3. R Beattie, S Hippenmeyer, Mechanisms of radial glia progenitor cell lineage progression. *FEBS Lett.* **591**, 3993–4008 (2017).
4. E Taverna, M Götz, WB Huttner, The cell biology of neurogenesis: toward an understanding of the development and evolution of the neocortex. *Annu. Rev. Cell Dev. Biol.* **30**, 465–502 (2014).

5. K Frederiksen, RD McKay, Proliferation and differentiation of rat neuroepithelial precursor cells in vivo. *The J. Neurosci.* **8**, 1144–1151 (1988).
6. E Hartfuss, R Galli, N Heins, M Götz, Characterization of CNS precursor subtypes and radial glia. *Dev. Biol.* **229**, 15–30 (2001).
7. T Miyata, A Kawaguchi, H Okano, M Ogawa, Asymmetric inheritance of radial glial fibers by cortical neurons. *Neuron* **31**, 727–741 (2001).
8. SC Noctor, V Martínez-Cerdeño, L Ivic, AR Kriegstein, Cortical neurons arise in symmetric and asymmetric division zones and migrate through specific phases. *Nat. Neurosci.* **7**, 136–144 (2004).
9. R Losick, C Desplan, Stochasticity and cell fate. *Science* **320**, 65–68 (2008).
10. J Teles, et al., Transcriptional regulation of lineage commitment–a stochastic model of cell fate decisions. *PLoS Comput. Biol.* **9**, e1003197 (2013).
11. CE Müller-Sieburg, RH Cho, M Thoman, B Adkins, HB Sieburg, Deterministic regulation of hematopoietic stem cell self-renewal and differentiation. *Blood* **100**, 1302–1309 (2002).
12. Y Kosodo, et al., Asymmetric distribution of the apical plasma membrane during neurogenic divisions of mammalian neuroepithelial cells. *The EMBO J.* **23**, 2314–2324 (2004).
13. WB Huttner, Y Kosodo, Symmetric versus asymmetric cell division during neurogenesis in the developing vertebrate central nervous system. *Curr. Opin. Cell Biol.* **17**, 648–657 (2005).
14. DG Míguez, A branching process to characterize the dynamics of stem cell differentiation. *Sci. reports* **5**, 13265 (2015).
15. J He, et al., How variable clones build an invariant retina. *Neuron* **75**, 786–798 (2012).
16. Z Chen, X Li, C Desplan, Deterministic or stochastic choices in retinal neuron specification. *Neuron* **75**, 739–742 (2012).
17. E Clayton, et al., A single type of progenitor cell maintains normal epidermis. *Nature* **446**, 185–189 (2007).
18. VH Teixeira, et al., Stochastic homeostasis in human airway epithelium is achieved by neutral competition of basal cell progenitors. *eLife* **2**, e00966 (2013).
19. AM Klein, T Nakagawa, R Ichikawa, S Yoshida, BD Simons, Mouse germ line stem cells undergo rapid and stochastic turnover. *Cell Stem Cell* **7**, 214–224 (2010).
20. HJ Snippert, et al., Intestinal crypt homeostasis results from neutral competition between symmetrically dividing lgr5 stem cells. *Cell* **143**, 134–144 (2010).
21. P Gao, et al., Deterministic progenitor behavior and unitary production of neurons in the neocortex. *Cell* **159**, 775–788 (2014).
22. L Cai, NL Hayes, T Takahashi, VS Caviness, RS Nowakowski, Size distribution of retrovirally marked lineages matches prediction from population measurements of cell cycle behavior. *J. Neurosci. Res.* **69**, 731–744 (2002).
23. X Qian, et al., Timing of CNS cell generation. *Neuron* **28**, 69–80 (2000).
24. LGW Hilgenberg, MA Smith, Preparation of dissociated mouse cortical neuron cultures. *J. Vis. Exp.*, 562 (2007).
25. X Qian, AA Davis, SK Goderie, S Temple, FGF2 concentration regulates the generation of neurons and glia from multipotent cortical stem cells. *Neuron* **18**, 81–93 (1997).
26. P Oberst, et al., Temporal plasticity of apical progenitors in the developing mouse neocortex. *Nature* **573**, 370–374 (2019).
27. RS Nowakowski, SB Lewin, MW Miller, Bromodeoxyuridine immunohistochemical determination of the lengths of the cell cycle and the DNA-synthetic phase for an anatomically defined population. *J. Neurocytol.* **18**, 311–318 (1989).
28. A Salic, TJ Mitchison, A chemical method for fast and sensitive detection of DNA synthesis in vivo. *Proc. Natl. Acad. Sci. United States Am.* **105**, 2415–2420 (2008).
29. SB Buck, et al., Detection of s-phase cell cycle progression using 5-ethynyl-2'-deoxyuridine incorporation with click chemistry, an alternative to using 5-bromo-2'-deoxyuridine antibodies. *Biotechniques* **44**, 927–929 (2008).
30. MR Alexiades, C Cepko, Quantitative analysis of proliferation and cell cycle length during development of the rat retina. *Dev. Dyn.* **205**, 293–307 (1996).
31. M Takahashi, Theoretical basis for cell cycle analysis i. labelled mitosis wave method. *J. Theor. Biol.* **13**, 202–211 (1966).
32. T Takahashi, RS Nowakowski, VS Caviness, The leaving or q fraction of the murine cerebral proliferative epithelium: a general model of neocortical neuronogenesis. *The J. Neurosci.* **16**, 6183–6196 (1996).
33. PDM Macdonald, Statistical inference from the fraction labelled mitoses curve. *Biometrika* **57**, 489–503 (1970).
34. J Duque, N Gorfinkiel, Integration of actomyosin contractility with cell-cell adhesion during dorsal closure. *Development* **143**, 4676–4686 (2016).
35. LH Levkoff, et al., Bromodeoxyuridine inhibits cancer cell proliferation in vitro and in vivo. *Neoplasia* **10**, 804–816 (2008).
36. CB Johansson, et al., Identification of a neural stem cell in the adult mammalian central nervous system. *Cell* **96**, 25–34 (1999).
37. AC Begg, NJ McNally, DC Shrieve, H Kärcher, A method to measure the duration of DNA synthesis and the potential doubling time from a single sample. *Cytometry* **6**, 620–626 (1985).
38. M Hoyer, SM Bentzen, LN Salling, J Overgaard, Influence of sampling time on assessment of potential doubling time. *Cytometry* **16**, 144–151 (1994).
39. MC Johansson, B Baldetorp, PO Bendahl, R Johansson, SM Oredsson, An improved mathematical method to estimate DNA synthesis time of bromodeoxyuridine-labelled cells, using FCM-derived data. *Cell Prolif.* **27**, 475–488 (1994).
40. TS Weber, I Jaehnert, C Schichor, M Or-Guil, J Carneiro, Quantifying the length and variance of the eukaryotic cell cycle phases by a stochastic model and dual nucleoside pulse labelling. *PLoS Comput. Biol.* **10**, e1003616 (2014).
41. HY Lee, AS Perelson, Modeling t cell proliferation and death in vitro based on labeling data: generalizations of the smith-martin cell cycle model. *Bull. Math. Biol.* **70**, 21–44 (2008).
42. A Zilman, VV Ganusov, AS Perelson, Stochastic models of lymphocyte proliferation and death. *Plos One* **5**, e12775 (2010).
43. MA Ritter, JF Fowler, Y Kim, MJ Lindstrom, TJ Kinsella, Single biopsy, tumor kinetic analyses: A comparison of methods and an extension to shorter sampling intervals. *Int. J. Radiat. Oncol.* **23**, 811–820 (1992).
44. P Taupin, BrdU immunohistochemistry for studying adult neurogenesis: paradigms, pitfalls, limitations, and validation. *Brain Res. Rev.* **53**, 198–214 (2007).
45. S Shibui, T Hoshino, M Vanderlaan, JW Gray, Double labeling with iodo- and bromodeoxyuridine for cell kinetics studies. *The J. Histochem. Cytochem.* **37**, 1007–1011 (1989).
46. M Saade, et al., Sonic hedgehog signaling switches the mode of division in the developing nervous system. *Cell reports* **4**, 492–503 (2013).
47. G Le Dréau, M Saade, I Gutiérrez-Vallejo, E Martí, The strength of SMAD1/5 activity determines the mode of stem cell division in the developing spinal cord. *The J. Cell Biol.* **204**, 591–605 (2014).
48. T Takahashi, RS Nowakowski, VS Caviness, The cell cycle of the pseudostratified ventricular epithelium of the embryonic murine cerebral wall. *The J. Neurosci.* **15**, 6046–6057 (1995).
49. F Calegari, WB Huttner, An inhibition of cyclin-dependent kinases that lengthens, but does not arrest, neuroepithelial cell cycle induces premature neurogenesis. *J. Cell Sci.* **116**, 4947–4955 (2003).
50. F Calegari, W Haubensak, C Haffner, WB Huttner, Selective lengthening of the cell cycle in the neurogenic subpopulation of neural progenitor cells during mouse brain development. *The J. Neurosci.* **25**, 6533–6538 (2005).
51. C Dehay, H Kennedy, Cell-cycle control and cortical development. *Nat. Rev. Neurosci.* **8**, 438–450 (2007).
52. G Mairet-Coello, et al., p57(KIP2) regulates radial glia and intermediate precursor cell cycle dynamics and lower layer neurogenesis in developing cerebral cortex. *Development* **139**, 475–487 (2012).
53. M Roccio, et al., Predicting stem cell fate changes by differential cell cycle progression patterns. *Development* **140**, 459–470 (2013).
54. Y Arai, et al., Neural stem and progenitor cells shorten s-phase on commitment to neuron production. *Nat. Commun.* **2**, 154 (2011).
55. A Iulianella, M Sharma, M Durnin, GB Vanden Heuvel, PA Trainor, Cux2 (cutl2) integrates neural progenitor development with cell-cycle progression during spinal cord neurogenesis. *Development* **135**, 729–741 (2008).
56. M Locker, et al., Hedgehog signaling and the retina: insights into the mechanisms controlling the proliferative properties of neural precursors. *Genes & Dev.* **20**, 3036–3048 (2006).
57. EF Juarez, et al., Quantifying differences in cell line population dynamics using CellPD. *BMC Syst. Biol.* **10**, 92 (2016).
58. DM Suter, D Tirefort, S Julien, KH Krause, A sox1 to pax6 switch drives neuroectoderm to radial glia progression during differentiation of mouse embryonic stem cells. *Stem Cells* **27**, 49–58 (2009).
59. GE Elsen, et al., The epigenetic factor landscape of developing neocortex is regulated by transcription factors pax6, tbr2, tbr1. *Front. Neurosci.* **12**, 571 (2018).
60. BJ Molyneaux, P Arlotta, JRL Menezes, JD Macklis, Neuronal subtype specification in the cerebral cortex. *Nat. Rev. Neurosci.* **8**, 427–437 (2007).
61. SR Hutton, LH Pevny, SOX2 expression levels distinguish between neural progenitor populations of the developing dorsal telencephalon. *Dev. Biol.* **352**, 40–47 (2011).
62. W Kang, LC Wong, SH Shi, JM Hébert, The transition from radial glial to intermediate progenitor cell is inhibited by FGF signaling during corticogenesis. *The J. Neurosci.* **29**, 14571–14580 (2009).
63. S Bouleau, et al., FGF1 inhibits p53-dependent apoptosis and cell cycle arrest via an intracrine pathway. *Oncogene* **24**, 7839–7849 (2005).
64. A Sigal, et al., Variability and memory of protein levels in human cells. *Nature* **444**, 643–646 (2006).
65. O Sandler, et al., Lineage correlations of single cell division time as a probe of cell-cycle dynamics. *Nature* **519**, 468–471 (2015).
66. G Mairet-Coello, A Tury, E DiCicco-Bloom, Insulin-like growth factor-1 promotes g(1)/s cell cycle progression through bidirectional regulation of cyclins and cyclin-dependent kinase inhibitors via the phosphatidylinositol 3-kinase/akt pathway in developing rat cerebral cortex. *The J. Neurosci.* **29**, 775–788 (2009).
67. RD Hodge, AJ D'Ercole, JR O'Kusky, Insulin-like growth factor-i accelerates the cell cycle by decreasing g1 phase length and increases cell cycle reentry in the embryonic cerebral cortex. *The J. Neurosci.* **24**, 10201–10210 (2004).
68. H Harrison, HJ Pegg, J Thompson, C Bates, P Shore, HIF1-alpha expressing cells induce a hypoxic-like response in neighbouring cancer cells. *BMC Cancer* **18**, 674 (2018).

DRAFT